ChemComm

ROYAL SOCIETY OF CHEMISTRY

COMMUNICATION

View Article Online
View Journal | View Issue

Cite this: *Chem. Commun.*, 2023, **59**, 3095

Received 21st December 2022,
Accepted 15th February 2023

DOI: 10.1039/d2cc06953a

rsc.li/chemcomm

White emission in 3D-printed phosphor microstructures†

Jędrzej Winczewski, *[a] Manuel Herrera,[b] Han Gardeniers [a] and Arturo Susarrey-Arce *[a]

Microscale functional materials permit advanced applications in optics and photonics. This work presents the additive manufacturing of three-dimensional structured phosphors emitting red, green, blue, and white. The development is a step forward to realizing additive colour synthesis within complex architectures of relevance in integrated optics or light-emitting sources.

Two-photon lithography (TPL) has unfolded as a buoyant methodology permitting the fabrication of complex three-dimensional (3D) structures with sub-micrometer resolution.[1] In standard microscope-based TPL systems, femtosecond laser radiation is utilized to initiate the photopolymerization within the focal point, which position is scanned to solidify the negative-tone photoresin into the desired 3D shapes (Fig. 1).[1] TPL is often used with other fabrication approaches to exploit the full potential, as the intrinsic properties of the standard organic photoresins offer a limited range of applications. Recently, alternatives to standard organic photoresins based on simple monomeric species have been developed. Besides the polymers of modified functionalities, the materials manufactured using the tailor-made photoresins include, *e.g.*, metals, ceramics, or nanocomposites.[2–4] The pre-ceramic photoresins have reached increasing recognition attributed to their technological importance and the versatile characteristics of the resulting materials, *e.g.*, piezoelectricity, and high mechanical strength.[3,5,6] Examples of 3D-structured ceramic microstructures include, *i.e.* ZnO, TiO_2, and ZrO_2.[3,5,6] Due to their high chemical and physical stability, resistance to continuous excitation, and high lattice-binding energies, ceramics are often the host matrices of choice for rare-earth ions (RE^{3+}).[7] Upon excitation, phosphorous materials are highly-efficient emitters of narrowly defined radiation that find a broad range of applications, such as microoptics.[8] Low phonon energy ceramics are typically preferred, as they promote higher RE^{3+} optical transitions quantum efficiencies by reducing non-radiative decay rates.[9] Sufficient RE^{3+} solubility is required to prevent dopant clustering.[9] ZrO_2 fulfils the above considerations and has frequently been applied as a RE^{3+} host. The rationale is that the microscale 3D structuring of phosphors may grant measures for mitigating thermal quenching *via* optimized heat dissipation or restraining the optical crosstalk.[10] Various forms of structured ZrO_2 phosphors have been manufactured, *i.e.*, nanotube arrays, nanofibers, or macro-mesoporous structures.[11–13] Recently, we presented an alternative methodology for fabricating compound 3D ZrO_2:Eu^{3+} microstructures emitting in orange-red.[10] The development of 3D phosphors emitting in other primary colours and white is a step forward to realizing additive colour synthesis within complex architectures of relevance in integrated optics or light-emitting sources.[8] Further, the biocompatibility of ZrO_2 could also prospectively permit their use in biomedical imaging or sensing.[14,15]

In this study, we present the additive manufacturing (AM) of ZrO_2 doped structures emitting in red (Eu^{3+}), green (Tb^{3+}), blue (Tm^{3+}), and white (Eu^{3+}, Tb^{3+}, and Tm^{3+}). The method involves the preparation of tailor-made photoresins suitable for TPL, containing the Zr-rich acrylate monomer and acetate (Ac) salts

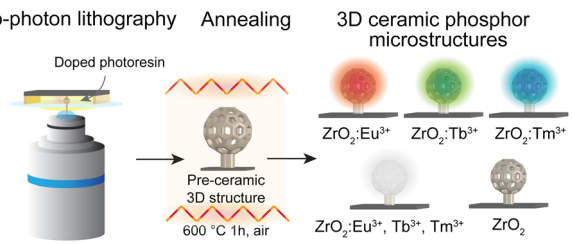

Fig. 1 Schematic simplified presentation of the AM of 3D pre-ceramic microstructures using tailor-made photoresists doped with RE^{3+} species and formation of ceramic replicas upon annealing at 600 °C for 1 h.

[a] *Mesoscale Chemical Systems, MESA+ Institute, University of Twente, P.O. Box 217, Enschede 7500 AE, The Netherlands. E-mail: j.p.winczewski@utwente.nl, a.susarreyarce@utwente.nl*

[b] *Centro de Nanociencias y Nanotecnología, Universidad Nacional Autónoma de México, Km 107 Carretera Tijuana-Ensenada, Ensenada, Baja California C.P. 22800, Mexico*

† Electronic supplementary information (ESI) available: Experimental details, supplementary figures. See DOI: https://doi.org/10.1039/d2cc06953a

of the lanthanides (Ln^{3+}). TPL is utilized to fabricate 3D architectures of arbitrary shapes from the custom-made photoresin. TPL has a miniaturization advantage, which is also a bottleneck regarding large-scale production. During the printing, the photoresin photopolymerizes, and both organic and metal–organic acrylates participate in the reaction, forming a metal–organic (pre-ceramic) polymer. In the photopolymer, and thus within the printed 3D structure, Ln^{3+} acetates are trapped, similar to the concept presented by Yee *et al.*[3] During the annealing, the organic constituents of the photopolymer (and the Ac groups of Ln^{3+} acetates) are combusted in the air. As a result, the metal–organic photopolymer is decomposed, the metallic part is oxidized, and the corresponding metal oxide (ZrO_2) is formed. Trivalent ions (*e.g.*, Ln^{3+}) can substitute Zr^{4+} ions in the ceramic matrix and act as dopants. The pre-ceramic architectures (in shape inspired by a C_{60} buckyball) printed on Si substrates are annealed at 600 °C for 1 h. After combustion, the doped ZrO_2 ceramics (ZrO_2:Ln^{3+}) is obtained, where Ln^{3+} is Eu^{3+}, Tb^{3+}, or Tm^{3+}. Additionally, triply-doped ZrO_2 is prepared with Eu^{3+}, Tb^{3+}, and Tm^{3+}. The doping is adjusted to 3 wt. % for the RE^{3+} species in ZrO_2:Ln^{3+}, and to 1 wt. % of each RE^{3+} species in the triply-doped material. The methodology is schematically depicted in Fig. 1. and described in the ESI† (S1.2).

The annealing promotes the formation of miniaturized ceramic replicas isotropically reduced in size by ≈ 60%. The result is shown in Fig. 2(a). Complimentary images of ZrO_2:Tb^{3+} and ZrO_2:Tm^{3+} gyroids and a ZrO_2:Eu^{3+}, Tb^{3+}, Tm^{3+} octet-truss lattice can be found in ESI† (Fig. S1). In Fig. 2(b–g), elemental mapping is conducted using Scanning Electron Microscopy-Energy Dispersive X-ray Spectroscopy (SEM-EDX), which confirms the uniform distribution of co-dopants throughout the ZrO_2 architecture. The O and Si signals are absent within the structural beams, and surface oxide on the Si substrate is observed. The EDX spectrum (Fig. 2(i) features sharp O $K\alpha_1$, Si $K\alpha_1$ (substrate), and Zr Lα peaks centred at 0.52 eV, 1.74 eV, and 2.12 eV.[16] The insets present the signals originating from the RE^{3+} species. The Eu contributions are found at 1.14 eV ($M\alpha_1$), 5.85 eV ($L\alpha_1$), and 6.46 eV ($L\beta_1$).[16] Characteristic Tb peaks at 1.24 eV ($M\alpha_1$), 6.27 eV ($L\alpha_1$), and 6.98 eV ($L\beta_1$), and Tm signals at 1.46 eV ($M\alpha_1$), 7.18 eV ($L\alpha_1$), and 8.10 eV ($L\beta_1$) are also detected.[16] The analysis confirms the incorporation of Eu, Tb, and Tm within the ZrO_2 structure. The site symmetry and structure influence the radiative transitions of the hosted RE^{3+} ions.[17] The crystallographic phase of the undoped and doped ZrO_2 is assessed with X-ray diffraction (XRD) (Fig. S3, ESI†) and cross-checked with confocal Raman spectroscopy (Raman) (Fig. S4, ESI†). In short, for XRD and Raman, tetragonal zirconia (t-ZrO_2) is observed for the doped ZrO_2. The estimated crystallite sizes are approximately 7 nm (S.4.1., ESI†). Four intense Raman modes are detected at 145 cm^{-1} (B_{1g}), 267 cm^{-1} (E_g), 462 cm^{-1} (E_g), and 646 cm^{-1} (E_g) with weaker shoulders at 316 cm^{-1} (B_{1g}), and 606 cm^{-1} (B_{1g}) for the undoped t-ZrO_2 microstructure.[18–20] All these vibrational modes are also observed for ZrO_2 doped with Eu^{3+}, Tb^{3+}, and Tm^{3+}, and ZrO_2 co-doped with Eu^{3+}, Tb^{3+}, and Tm^{3+}. The results agree with the literature on ZrO_2 doped with ≈ 3 wt% of Ln^{3+} species and with our previous work.[10,21] In a previous study employing X-ray photoelectron spectroscopy, we confirmed the predominant oxidation state of Eu species introduced into the ZrO_2 microstructures.[10] In the triply-doped ZrO_2, the Ln^{3+} loadings are low (≈ 1%), making it challenging to determine the species. Thus, we rely on the optical properties of the 3D structured ZrO_2, ZrO_2:Ln^{3+}, and ZrO_2:Eu^{3+}, Tb^{3+}, Tm^{3+} phosphors.

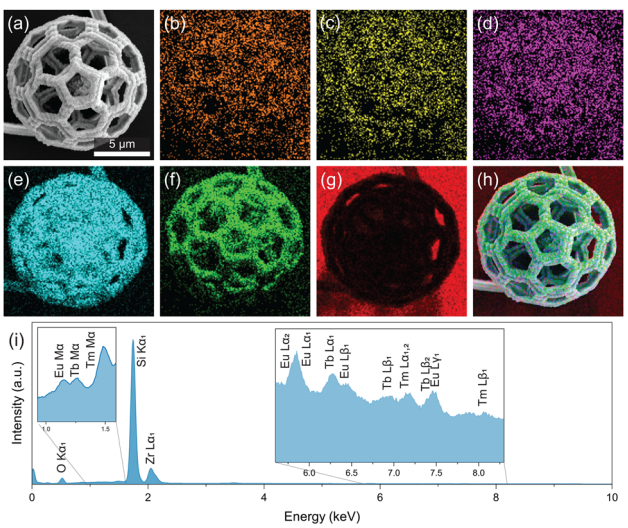

Fig. 2 (a) SEM image of the triply-doped ZrO_2 buckyball; (b–g) SEM-EDX elemental maps of (b) Eu, (c) Tb, (d) Tm, (e) Zr, (f) O, (g) Si, and (h) overlayed (a–g) images. (i) EDX spectrum collected from the ZrO_2:Ln^{3+} buckyball.

The optical properties of the 3D phosphor structures are investigated with cathodoluminescence (CL). Although differences in photoluminescence (PL) and CL spectra may occur, the microscale feature size of the architectures is the main reason for selecting the CL in this study.[22] The CL spectrum collected from the undoped t-ZrO_2 buckyball is a sum of Gaussian components at approximately 3.5 eV (356 nm), 3.2 eV (393 nm), 2.9 eV (434 nm), 2.6 eV (485 nm), and 2.3 eV (546 nm) (Fig. 3(a)), previously assigned to the F^+ centers, oxygen vacancies (V_O) and interstitial carbon (C_i) point-defects.[10] The spectra of ZrO_2 with a single RE^{3+} ion type reveal their characteristic transitions, significantly more intense than the negligible t-ZrO_2 CL components.[10] The CL spectrum of ZrO_2:Eu^{3+} is dominated by the sharp $^5D_0 \rightarrow {}^7F_1$ and $^5D_0 \rightarrow {}^7F_2$ (594 nm and 609 nm) and weak $^5D_0 \rightarrow {}^7F_2$ (≈628 nm) and $^5D_0 \rightarrow {}^7F_3$ (≈651 nm) transitions (Fig. 3(b)) are registered. The CL spectrum of ZrO_2:Tb^{3+} features the sharp $^5D_4 \rightarrow {}^7F_5$ (546 nm) line, medium-intensity $^5D_4 \rightarrow {}^7F_6$ (491 nm) emission, and weak $^5D_4 \rightarrow {}^7F_J$ (J = 4, 3) peaks (590 nm, 622 nm) (Fig. 3(c)).[23]

In the violet-blue spectral region, very weak emissions corresponding with $^5D_3 \rightarrow {}^7F_J$ transitions are detected (≈ 378 nm, 414 nm, and 436 nm).[23] The CL spectrum of ZrO_2:Tm^{3+} exhibits intense $^1D_2 \rightarrow {}^3F_4$ (459 nm), a medium intensity $^1D_2 \rightarrow {}^3H_6$ line (359 nm), and a very weak $^1G_4 \rightarrow {}^3F_4$ (≈ 648 nm) transition (Fig. 3(d)).[21,24] The co-doping of ZrO_2 with Eu^{3+}, Tb^{3+}, and Tm^{3+} results in distinctive individual contributions and signals related to energy transfer (ET) interactions (Fig. 3(e)). The sharp Eu^{3+} $^5D_0 \rightarrow {}^7F_1$ (≈590 nm) and $^5D_0 \rightarrow {}^7F_2$ (≈ 606 nm)

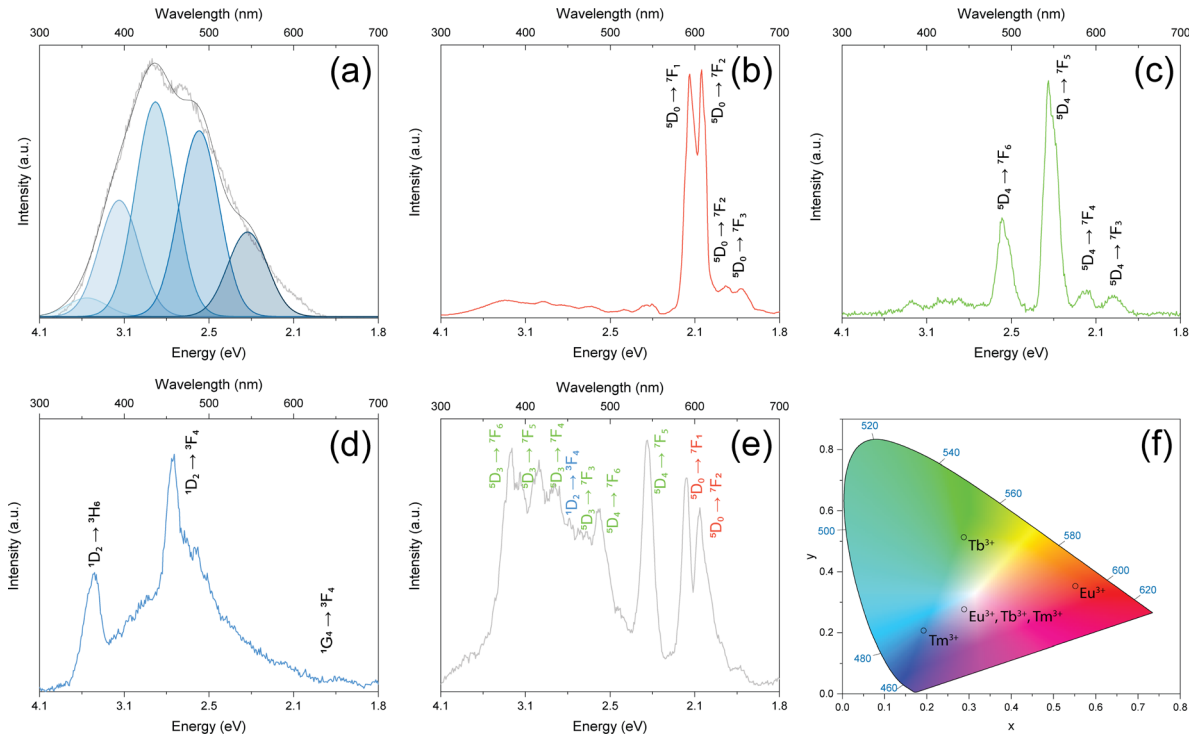

Fig. 3 CL spectra registered for the buckyballs: (a) ZrO_2, (b) ZrO_2:Eu^{3+}, (c) ZrO_2:Tb^{3+}, (d) ZrO_2:Tm^{3+}, and (e) ZrO_2 triply-doped with Eu^{3+}, Tb^{3+}, and Tm^{3+}, and (f) 1931 CIE chromaticity diagram with labels corresponding to the RE^{3+} dopants in ZrO_2.

emission lines, and weaker $^5D_0 \rightarrow {}^7F_2$ ($\approx$ 626 nm) and $^5D_0 \rightarrow {}^7F_3$ ($\approx$ 651 nm) transitions. The distinct Tb^{3+} $^5D_4 \rightarrow {}^7F_5$ and $^5D_4 \rightarrow {}^7F_6$ transitions are also observed. Several contributions can be assigned within the 360–460 nm region, including the overlapped Tm^{3+} $^1D_2 \rightarrow {}^3F_4$ (459 nm) transition. The sharp Tm^{3+} emissions cannot unambiguously be distinguished.[21] The suppression of the Tm^{3+} $^1D_2 \rightarrow {}^3H_6$ transition (observed around 359 nm in the ZrO_2:Tm^{3+} spectrum) and accompanying appeareance of Tb^{3+} $^5D_3 \rightarrow {}^7F_J$ emissions may imply the ET from the Tm^{3+} $^1D_2$ level to Tb^{3+} $^5D_3$ level, likely involving a relaxation.[21,22,25] Consistently, several intense Tb^{3+} transitions ($^5D_3 \rightarrow {}^7F_{6,5,4,3}$) are observed ($\approx$ 380 nm, 410 nm, 440 nm, and 460 nm), which have previously been reported at low Tb^{3+} ($\approx$ 2 at%) concentrations in $LiLuF_4$ under 353 nm excitation.[22] At lower Tb^{3+} concentrations, the probability of cross-relaxation decreases, promoting the $^5D_3 \rightarrow {}^7F_J$ transitions.[26] The effect is significant at low concentrations in the case of CL spectra but not observed in the case of PL.[26,27] The blue emission has been proposed to be correlated with the presence of Tb^{4+} ions, which can substitute the Zr^{4+} ion positions. Upon the impact of electrons from the beam during CL measurements, Tb^{4+} ions can transiently be excited to the (Tb^{3+}) state and act as emissive centers.[27] Also, some of the excited electrons from the Tb^{3+} $^5D_4$ level may cross-relax to the Eu^{3+} $^5D_0$ level and contribute to the $^5D_0 \rightarrow {}^7F_0$, 1, 2 transitions.[21] We observe that the intensity of the $^5D_0 \rightarrow {}^7F_1$ transition is higher than the $^5D_0 \rightarrow {}^7F_2$ in the triply-doped sample. In principle, such an ET is very efficient due to the overlap of the Tm^{3+} $^5D_4 \rightarrow {}^7F_{6,5,4,3}$ emissions and the Eu^{3+} $^7F_{0,1} \rightarrow {}^5D_0$, 1, 2 absorptions.[21] The PL from the RE^{3+} is indirectly confirmed by exciting it at 532 nm, using Raman system and Eu^{3+} as an example. A similar concept has previously been presented by Tiseanu *et al.* (Fig. S5, ESI†).[28]

The CL spectra are converted into the Commission Internationale de l'éclairage (CIE) 1931 color space chromaticity diagram (Fig. 3(f)). The CIE coordinates might slightly differ from their respective PL emissions, as the ET may be less apparent in the case of the electron beam excitation when compared with the ultraviolet pump.[22] The CIE coordinates of single-doped ZrO_2 fall into the orange-red (Eu^{3+}), green (Tb^{3+}), and blue (Tm^{3+}) regions. The triple doping (Eu^{3+}, Tb^{3+}, and Tm^{3+}) promotes white emission (Fig. 3(f)). Although the main goal of this study is to present the white emission in triply-doped microstructures, additional insights into the effect of high-temperature annealing (1200 °C for 1 and 3 h) on the optical properties of ZrO_2:Eu^{3+}, ZrO_2:Tb^{3+}, ZrO_2:Tm^{3+}, and ZrO_2:Eu^{3+}, Tb^{3+}, Tm^{3+} architectures are provided (Fig. S6, ESI†). Complimentary SEM images of the buckyballs annealed at 1200 for 3 h are also presented (Fig. S2, ESI†). The panchromatic CL image (Fig. 4(b)) presents the homogenous emission from the buckyball. The monochromatic CL images (Fig. 4(c–h)) are obtained at 3.24 eV, 2.99 eV, 2.55 eV, 2.28 eV, 2.10 eV, 2.05 eV to match the most intense transitions registered in the triply-doped sample, corresponding to the 383 nm, 415 nm, 486 nm, 544 nm, 594 nm, and 605 nm in the visible range. Interestingly, CL images obtained at 3.24 eV, 2.99 eV, and 2.55 eV correspond to the transitions occurring mainly due to the ET, *e.g.*, $^5D_3 \rightarrow {}^7F_6$, or $^5D_3 \rightarrow {}^7F_5$, in which more uniform emission throughout the architecture is observed. Brighter regions are observed mainly at the edges of the architecture in the CL images

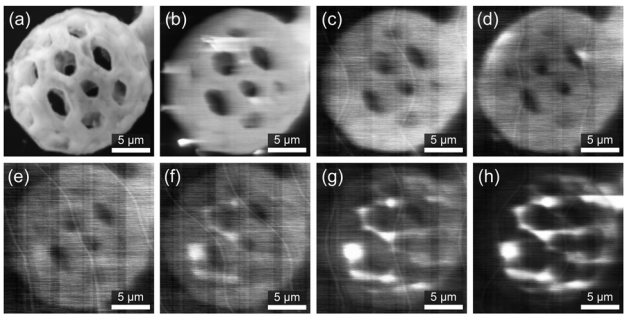

Fig. 4 Micrographs of the ZrO_2 buckyball doped with Eu^{3+}, Tb^{3+}, and Tm^{3+}; (a) SEM secondary electron image, (b) SEM panchromatic CL image, (c–h) monochromatic CL images at (c) 3.24 eV, (d) 2.99 eV, (e) 2.55 eV, (f) 2.28 eV, (g) 2.10 eV, and (h) 2.05 eV. Scale bars represent 5 μm.

obtained at 2.28 eV, 2.10 eV, and 2.05 eV, indicating possible Ln^{3+} segregation. Nevertheless, these regions can be associated with the most intense $^5D_4 \rightarrow {}^7F_5$ transition of ZrO_2:Tb^{3+} and $^5D_0 \rightarrow {}^7F_1$ and $^5D_0 \rightarrow {}^7F_2$ transitions of ZrO_2:Eu^{3+}.

In summary, we present tailor-made photoresins permitting the AM of microstructures doped with RE^{3+} species (Eu^{3+}, Tb^{3+}, Tm^{3+}) *via* TPL and subsequent annealing in the air. The thermal treatment of the 3D pre-ceramic structures results in forming ceramic replicas that are isometrically reduced in size by ≈60%. The incorporation of the RE^{3+} species within the ZrO_2 host is confirmed *via* SEM-EDX imaging. The *t*-ZrO_2 crystallographic phase of the fabricated ZrO_2:Ln^{3+} microstructures is confirmed using Raman spectroscopy. The coherent results are backed by XRD analysis of the reference ceramic powders obtained from the UV-cured photoresins annealed in bulk. The transitions of the ZrO_2:Ln^{3+} 3D structures are evaluated using CL, and according to the 1931 CIE colour space chromaticity diagram, the green (ZrO_2:Tb^{3+}), and blue (ZrO_2:Tm^{3+}) emissions are confirmed. The triple-doping promotes the ET from the Tm^{3+} to Tb^{3+} and from the Tb^{3+} to Eu^{3+}, and consequently, the white emission. The results show that the presented approach is suitable for the realization of complex 3D microarchitectures emitting close to all primary colours, and white.

J.P.W., A.S.-A., and H.G. are recipients of the Horizon 2020 ERC research and innovation programme of the European Union funding under Grant Agreement No. 742004. M.H. acknowledges support from the University of California Institute for Mexico and The United States (UCMEXUS) (No. CN19137) and CONACYT (Grant No. 284667).

Conflicts of interest

There are no conflicts to declare.

References

1 J. T. Fourkas, *Three-Dimensional Microfabrication Using Two-Photon Polymerization*, Elsevier Inc., Oxford, United Kingdom, 1st edn, 2016, ch. 1.3, pp. 57–76.
2 M. Carlotti and V. Mattoli, *Small*, 2019, **15**, 1902687.
3 D. W. Yee, M. L. Lifson, B. W. Edwards and J. R. Greer, *Adv. Mater.*, 2019, **31**, 1901345.
4 A. Vyatskikh, S. Delalande, A. Kudo, X. Zhang, C. M. Portela and J. R. Greer, *Nat. Commun.*, 2018, **9**, 593.
5 A. Vyatskikh, R. C. Ng, B. Edwards, R. M. Briggs and J. R. Greer, *Nano Lett.*, 2020, **20**, 3513–3520.
6 A. Desponds, A. Banyasz, D. Chateau, A. Tellal, A. Venier, S. Meille, G. Montagnac, J. Chevalier, C. Andraud, P. L. Baldeck and S. Parola, *Small*, 2021, **17**, 2102486.
7 J.-C. G. Bünzli, *Trends Chem.*, 2019, **1**, 751–762.
8 D. Gonzalez-Hernandez, S. Varapnickas, A. Bertoncini, C. Liberale and M. Malinauskas, *Adv. Opt. Mater.*, 2023, **11**, 2201701.
9 X. Chen, T. Sun and F. Wang, *Chem. – Asian J.*, 2020, **15**, 21–33.
10 J. Winczewski, M. Herrera, C. Cabriel, I. Izeddin, S. Gabel, B. Merle, A. Susarrey Arce and H. Gardeniers, *Adv. Opt. Mater.*, 2022, **10**, 2102758.
11 N. Fu, X. Wang, L. Guo, J. Zhao, X. Zhang, J. Lin, L. Gong, M. Wang and Y. Yang, *J. Mater. Sci.: Mater. Electron.*, 2017, **28**, 7253–7258.
12 A. B. Suryamas, M. M. Munir, T. Ogi, C. J. Hogan and K. Okuyama, *Jpn. J. Appl. Phys.*, 2010, **49**, 115003.
13 X. Qu, H. Song, X. Bai, G. Pan, B. Dong, H. Zhao, F. Wang and R. Qin, *Inorg. Chem.*, 2008, **47**, 9654–9659.
14 K. Soga, K. Tokuzen, K. Tsuji, T. Yamano, N. Venkatachalam, H. Hyodo and H. Kishimoto, *Opt. Compon. Mater. VII*, 2010, **7598**, 759807.
15 J. Wang, W. Yin, X. He, Q. Wang, M. Guo and S. Chen, *Sci. Rep.*, 2016, **6**, 35020.
16 J. B. Kortright and A. C. Thompson, in *X-ray Data Booklet*, ed. A. C. Thompson, Lawrence Berkeley National Laboratory, University of California, Berkeley, CA, USA, 3rd edn., 2009, pp. 8–27.
17 X. Chen, *Lanthanide-Doped Luminescent Nanomaterials*, Springer-Verlag, Heidelberg, Germany, 2014, ch. **5**, pp. 75–123.
18 G. Pezzotti and A. A. Porporati, *J. Biomed. Opt.*, 2004, **9**, 372.
19 X. Zhao and D. Vanderbilt, *Phys. Rev. B: Condens. Matter Mater. Phys.*, 2002, **65**, 075105.
20 A. P. Naumenko, N. I. Berezovska, M. M. Biliy and O. V. Shevchenko, *Phys. Chem. Solid State*, 2008, **9**, 121–125.
21 L. X. Lovisa, J. Andrés, L. Gracia, M. S. Li, C. A. Paskocimas, M. R. Bomio, V. D. Araujo, E. Longo and F. V. Motta, *J. Alloys Compd.*, 2017, **695**, 3094–3103.
22 S. Kalusniak, E. Castellano-Hernández, H. Yalçinoğlu, H. Tanaka and C. Kränkel, *Appl. Phys. B*, 2022, **128**, 33.
23 A. J. Silversmith, D. M. Boye, K. S. Brewer, C. E. Gillespie, Y. Lu and D. L. Campbell, *J. Lumin.*, 2006, **121**, 14–20.
24 A. A. El-Maaref, E. A. Wahab, K. S. Shaaban, M. Abdelawwad, M. S. Koubisy, J. Börcsök and E. S. Yousef, *Spectrochim. Acta, Part A*, 2020, **242**, 118774.
25 X. Xue, M. Thitsa, T. Cheng, W. Gao, D. Deng, T. Suzuki and Y. Ohishi, *Opt. Express*, 2016, **24**, 26307.
26 H. Seed Ahmed, O. Ntwaeaborwa, M. Gusowski, J. Botha and R. Kroon, *Phys. B: Condensed Matter*, 2012, **407**, 1653–1655.
27 M. Zawadzki, D. Hreniak, J. Wrzyszcz, W. Mišta, H. Grabowska, O. Malta and W. Stręk, *Chem. Phys.*, 2003, **291**, 275–285.
28 C. Tiseanu, B. Cojocaru, V. I. Parvulescu, M. Sanchez-Dominguez, P. A. Primus and M. Boutonnet, *Phys. Chem. Chem. Phys.*, 2012, **14**, 12970–12981.

